Supporting Information

Pt(IV) prodrug-gating MOF incorporating copper peroxide and ruthenium complex for NIR-mediated synergistic anticancer therapy

Romaine Parker,† Rajeshkumar Anbazhagan,† Chia-Yu Kuo, Teng-Hao Chen*

Institute of Clinical Pharmacy and Pharmaceutical Sciences, School of Pharmacy, College of Medicine, National Cheng Kung University, Tainan City 70101, Taiwan

*To whom correspondence should be addressed. E-mail: thchen@gs.ncku.edu.tw

† These authors contributed equally to this work.

Materials and Methods

Hydrogen peroxide (30%), zirconium chloride (99%), copper chloride (98%), and sodium hydroxide (99%) were purchased from Sigma-Aldrich. Succinic anhydride (99%), polyvinylpyrrolidone (99%), and cisplatin (99%) were purchased from Nova Materials Co., LTD. Acetic Acid (98%) and tris(2,2-bipyridyl) ruthenium (II) chloride hexahydrate (98%) were purchased from Thermo Fisher Scientific. Triethylamine (99%) was purchased from Tedia High Purity Solvents. N,N-Dimethylformamide (99%) and dimethyl sulfoxide (99%) were purchased from Macron Fin Chemicals. Ethanol (95%), dichloromethane, and acetone were purchased from Echo Chemical. Fourier transform infrared (FT-IR) spectroscopy data were collected on a PerkinElmer Frontier MIR Spectrometer. Powder X-ray diffraction (PXRD) patterns were collected on Bruker D8 Advance ECO with Cu Kα radiation. Scanning electron microscopy (SEM) images and energy dispersive X-ray spectroscopy (EDS) for elemental analysis were performed on SU8010 HR-FESEM. Zeta potential was measured on Beckman Coulter Delsa Nano C. Inductively coupled plasma atomic emission spectroscopy (ICP-AES) was performed on Thermo Scientific iCAP™ PRO. X-ray photoelectron spectroscopy (XPS) data were collected at room temperature using a ULVAC PHI 5000 VersaProbe III, equipped with an Al Kα (1487 eV) radiation source. The 3-(4,5-dimethyl thiazol-2-yl)-2,5-diphenyl tetrazolium bromide (MTT) assay absorbance was detected on the microplate reader SpectraMax i5x. The pH value measurements were taken using a Suntex SP-2100 pH meter. Oxygen generation was measured at Milwaukee MW600. The N_2 adsorption isotherms at 77 K were measured on a Micromeritics 3Flex Adsorption Analyzer.

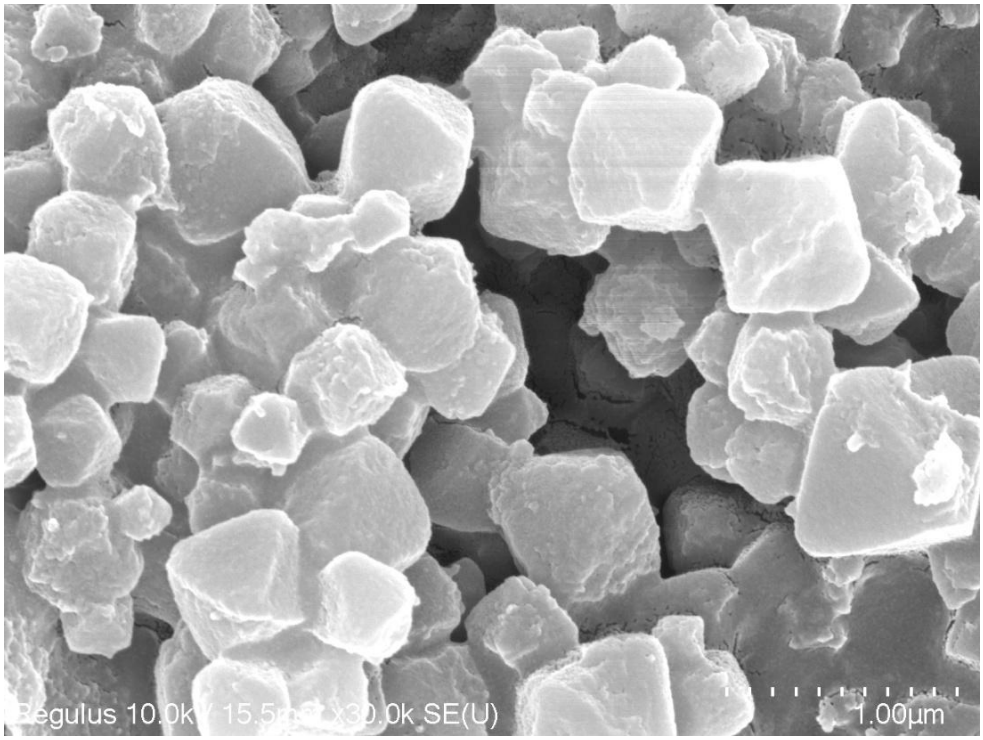

Fig. S1 SEM image of MOF.

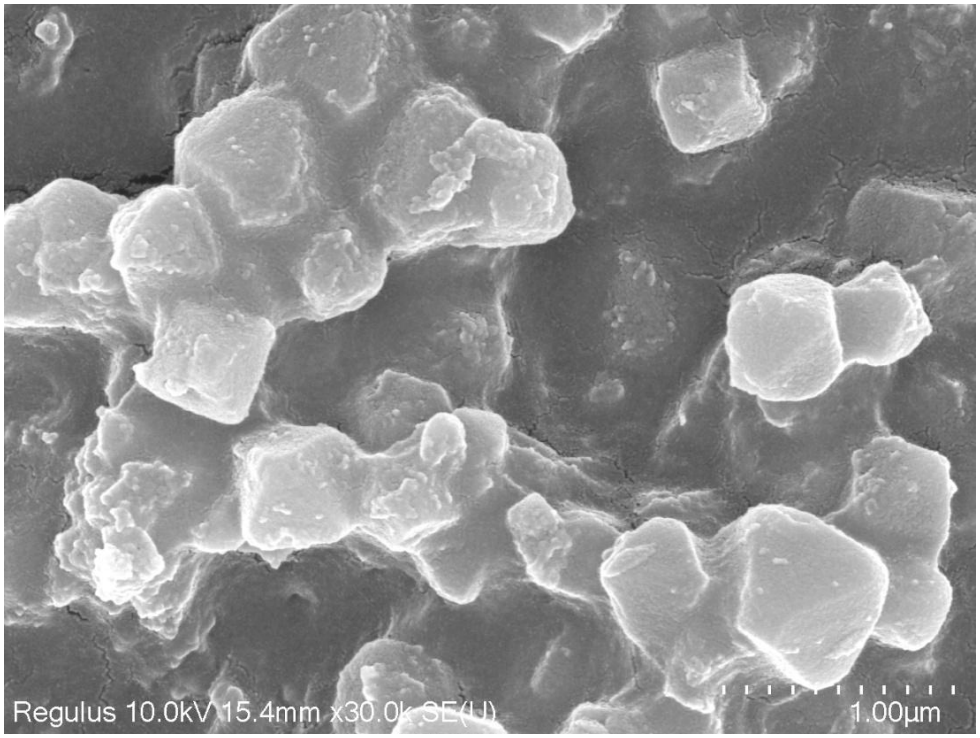

Fig. S2 SEM image of synthesized MOF@Cu.

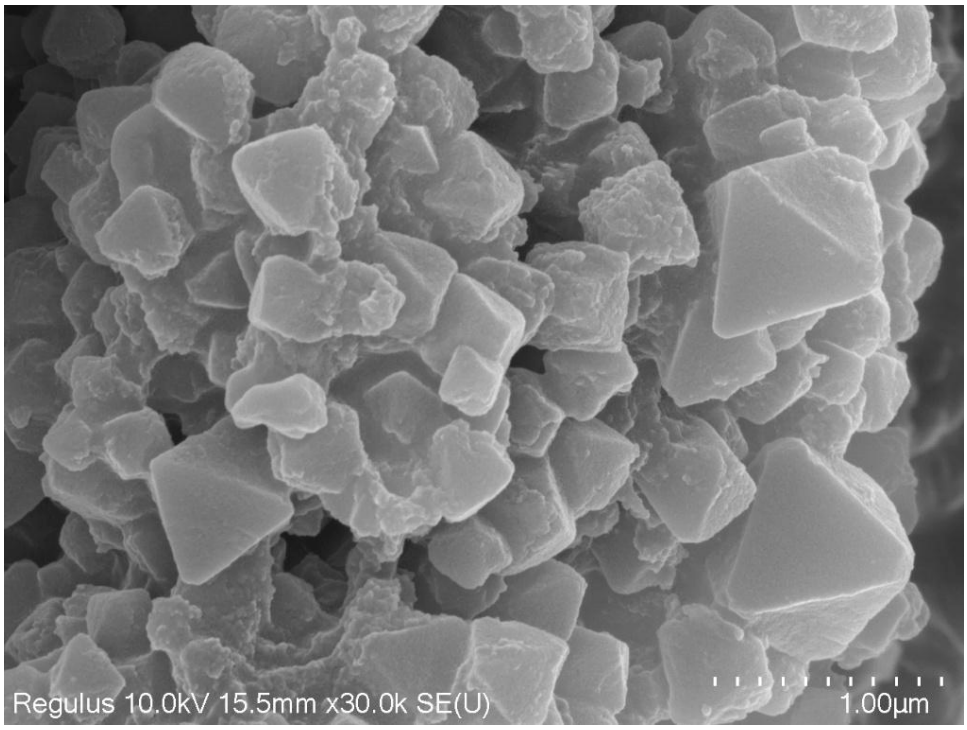

Fig. S3 SEM image of MOF@Cu/Ru.

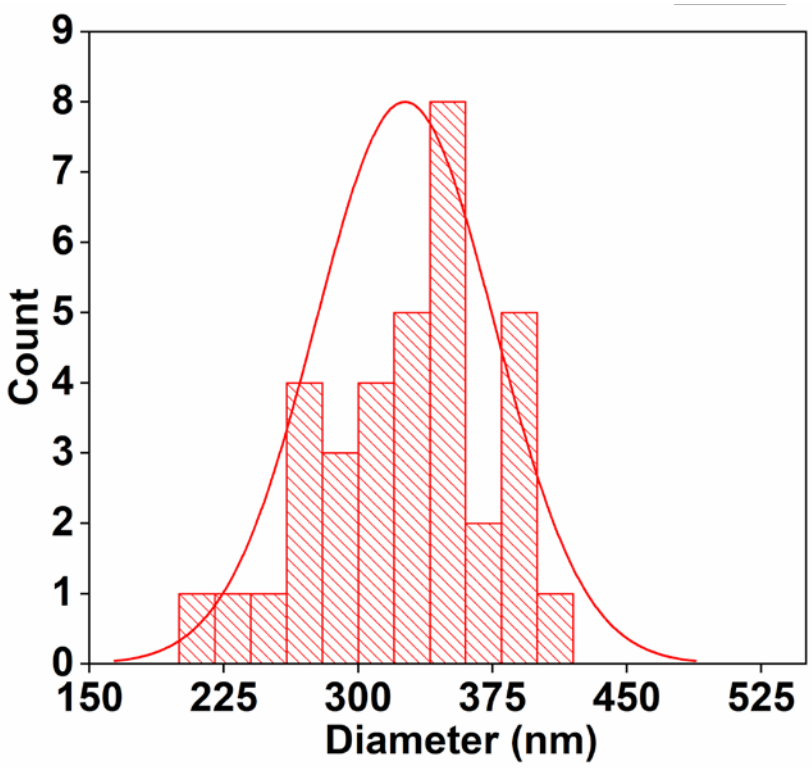

Fig. S4 The particle size distribution of MOF nanoparticles calculated from the SEM image.

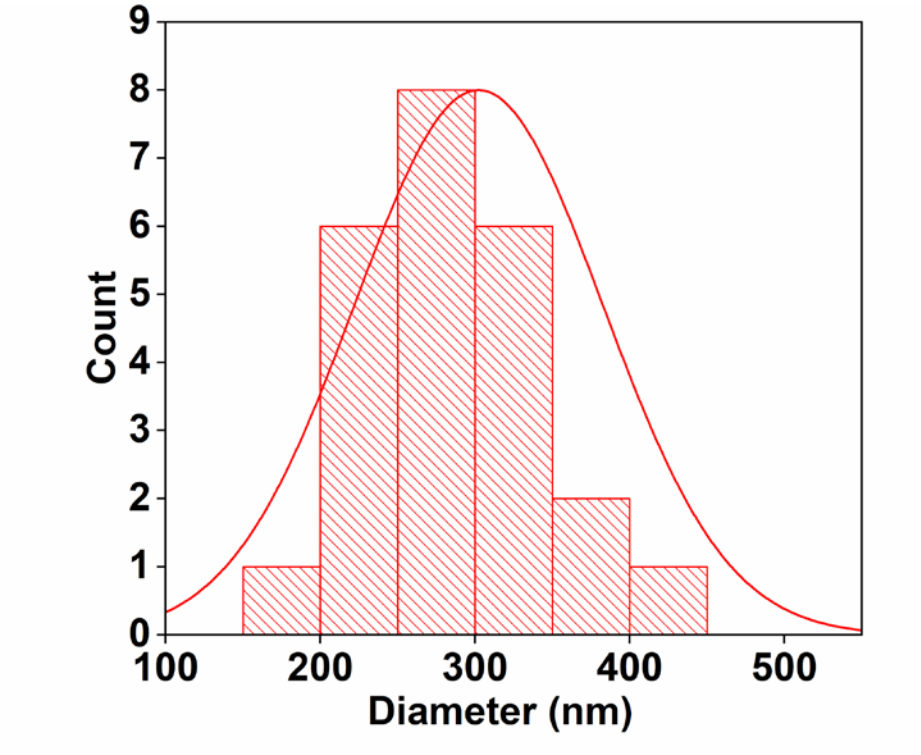

Fig. S5 The particle size distribution of MOF@Cu calculated from the SEM image.

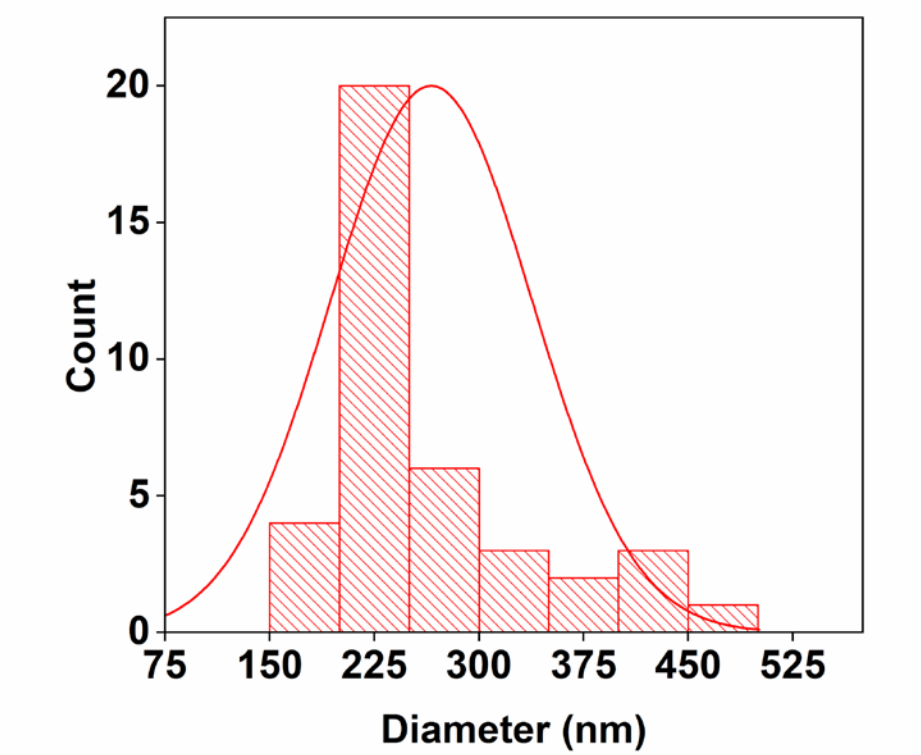

Fig. S6 The particle size distribution of MOF@Cu/Ru calculated from the SEM image.

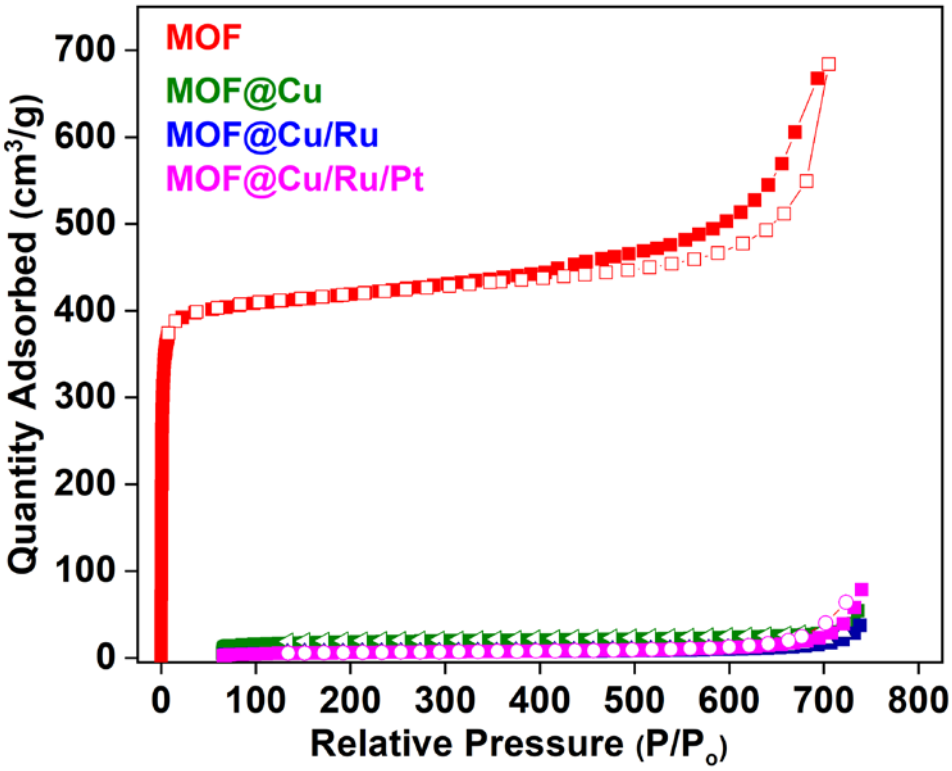

Fig. S7 Nitrogen sorption isotherms at 77 K for MOF, MOF@Cu, MOF@Cu/Ru, and MOF@Cu/Ru/Pt (filled: adsorption; empty: desorption).

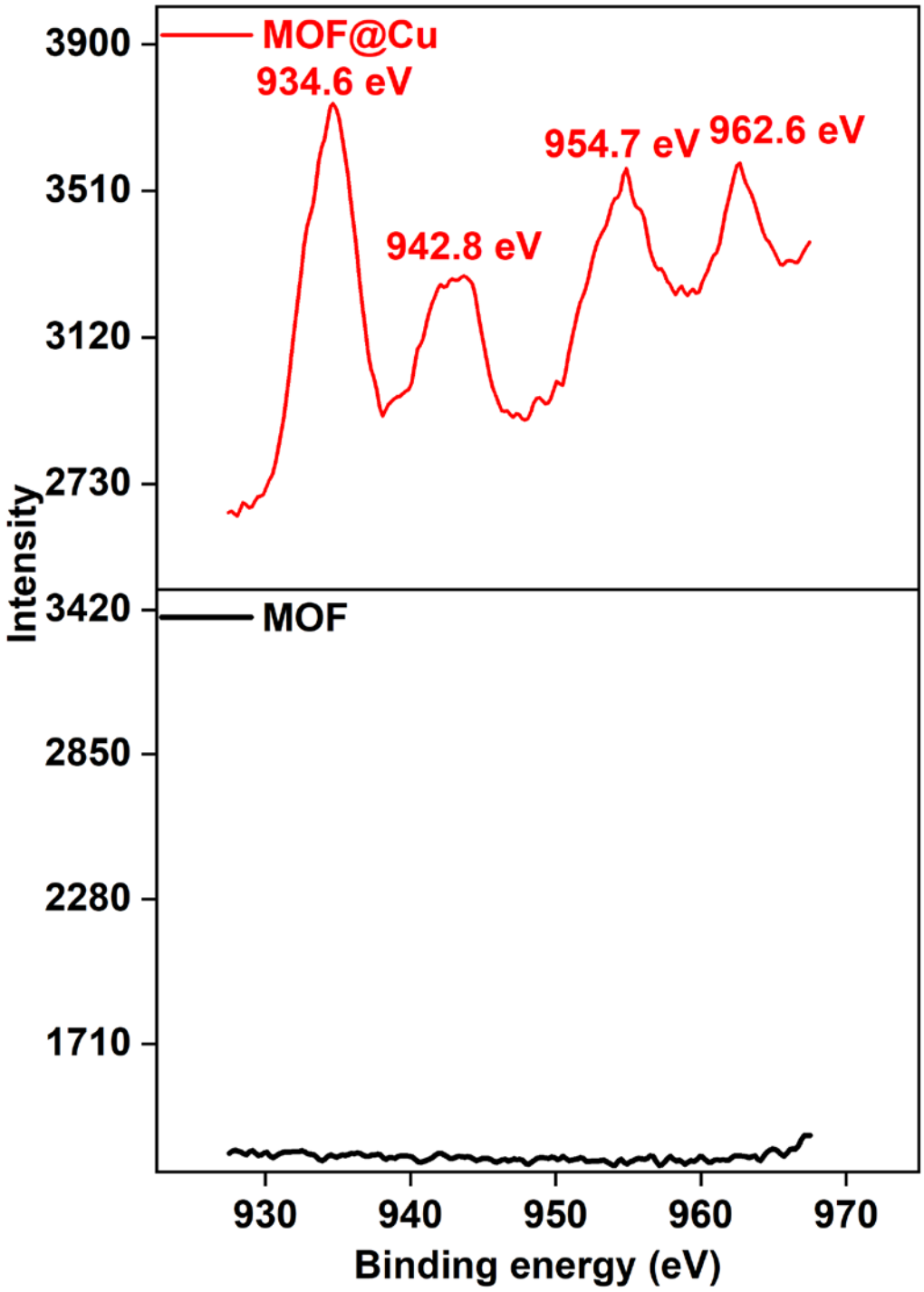

Fig. S8 Cu 2P XPS spectra of MOF and MOF@Cu.

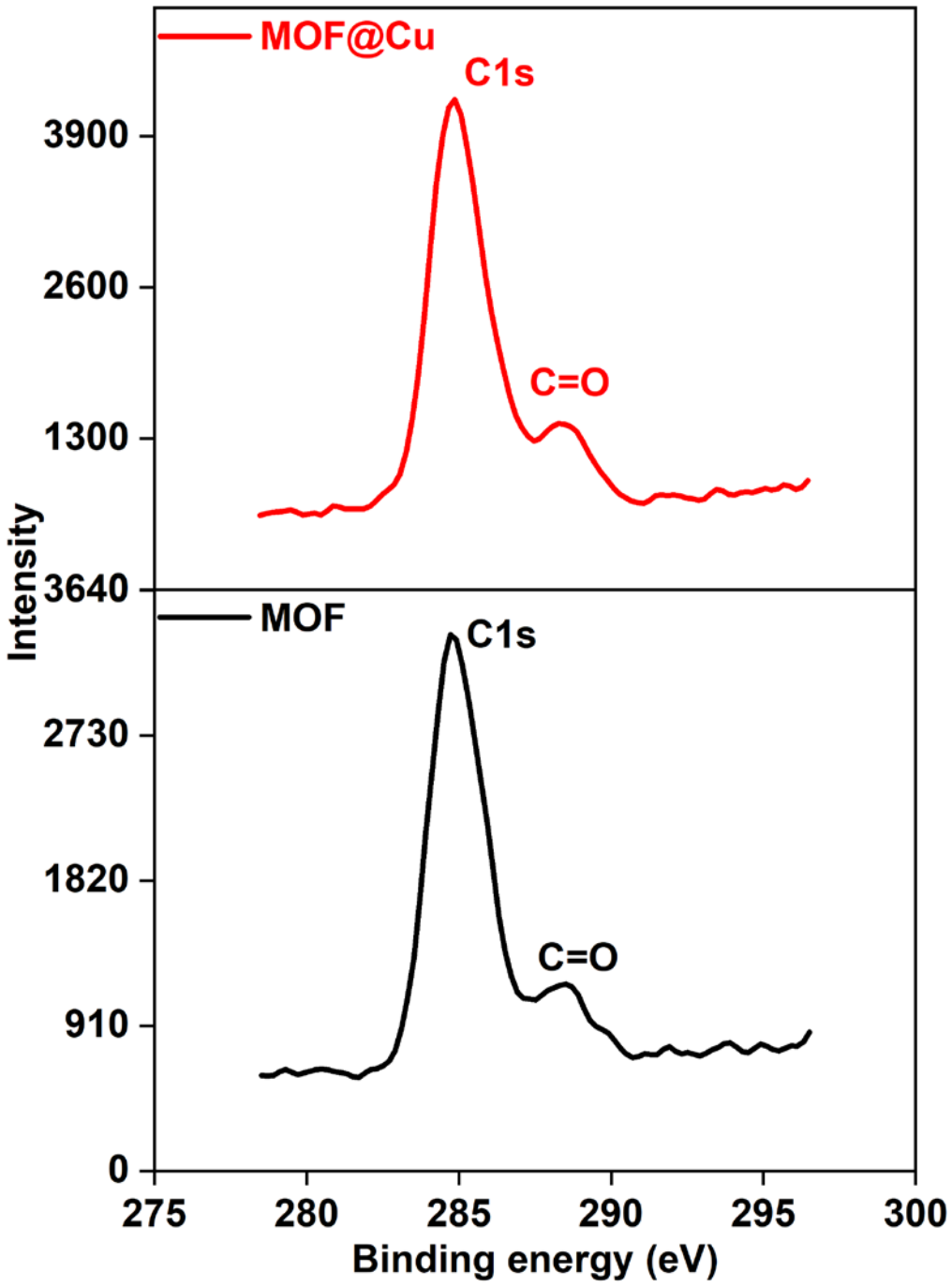

Fig. S9 C 1s XPS spectra of MOF and MOF@Cu.

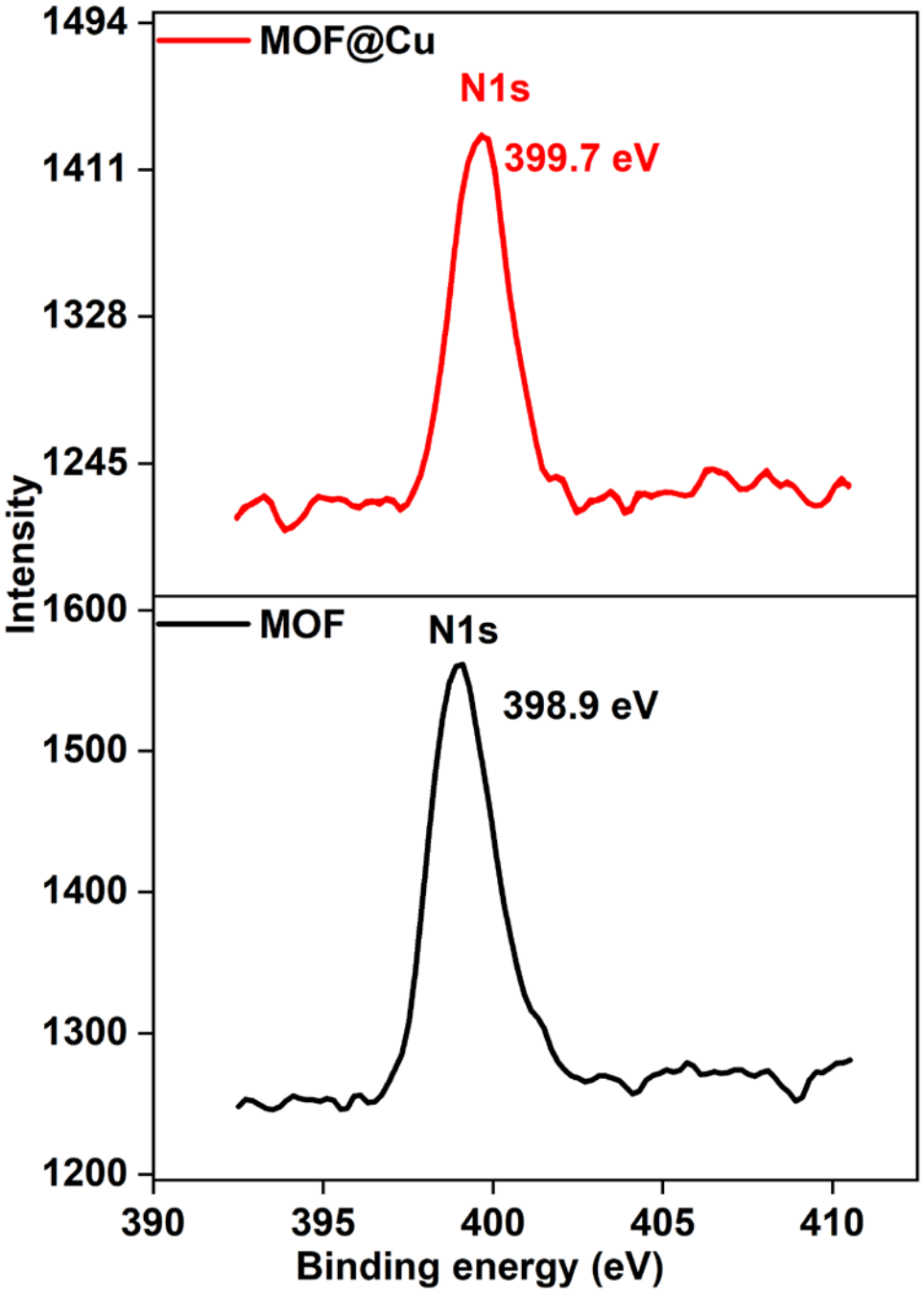

Fig. S10 N 1s XPS spectra of MOF and MOF@Cu.

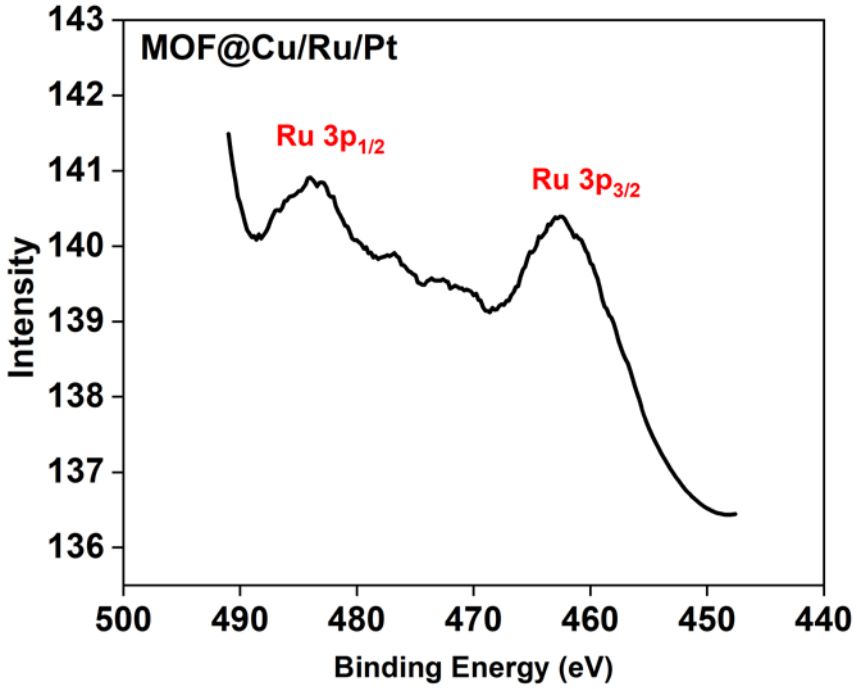

Fig. S11 Ru 3p XPS spectrum of MOF@Cu/Ru/Pt. The Ru 3p spectrum is used for analysis as the Ru 3d peak overlaps with the C 1s peak.

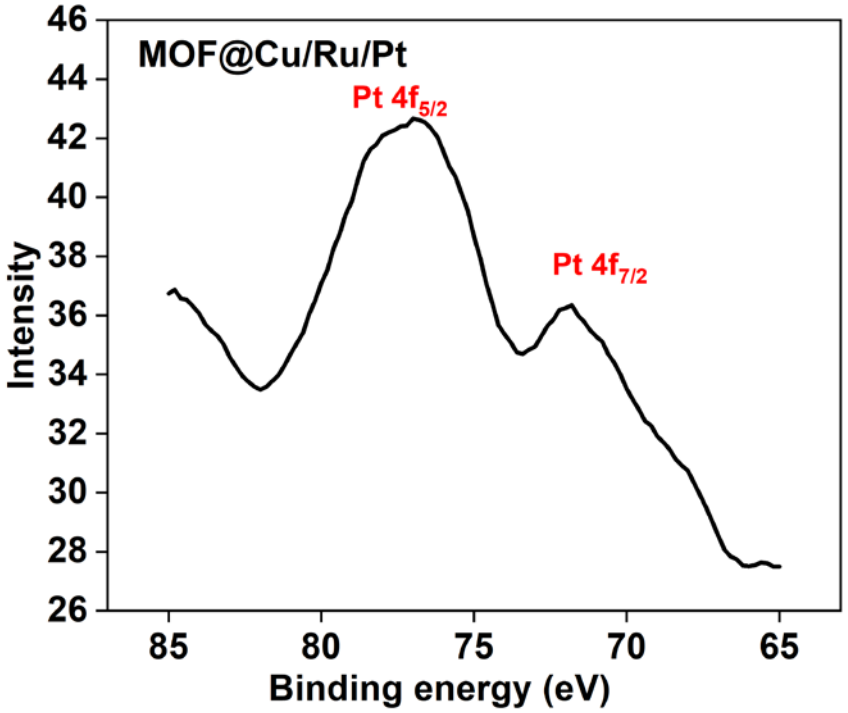

Fig. S12 Pt 4f XPS spectrum of MOF@Cu/Ru/Pt. A small amount of Pt(II) (Pt $4f_{7/2}$ binding energy at 71–73 eV) is observed, probably due to the photoactivation of Pt(IV) prodrug to Pt(II), in the presence of Ru(II) photosensitizer.[1]

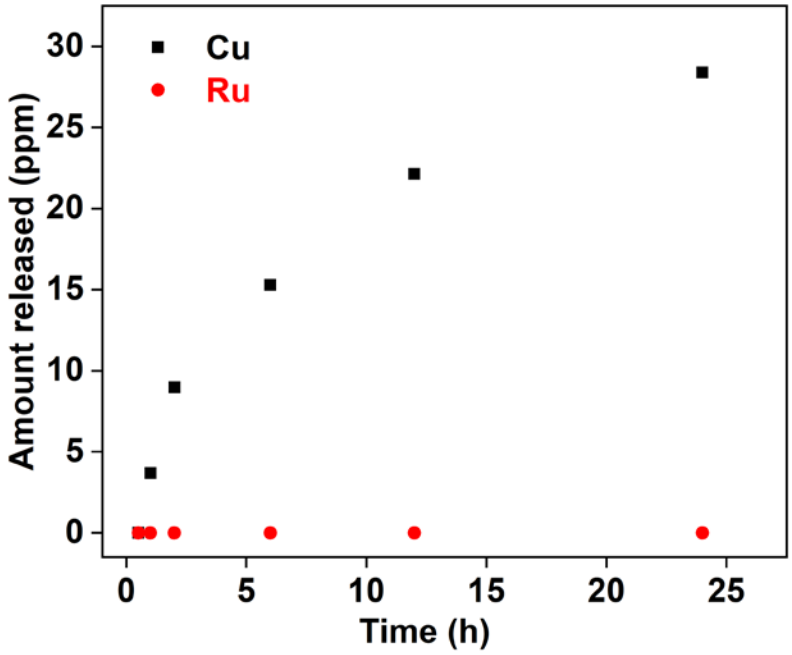

Fig. S13 Cu and Ru release of MOF@Cu/Ru in PBS solution (pH = 7.4).

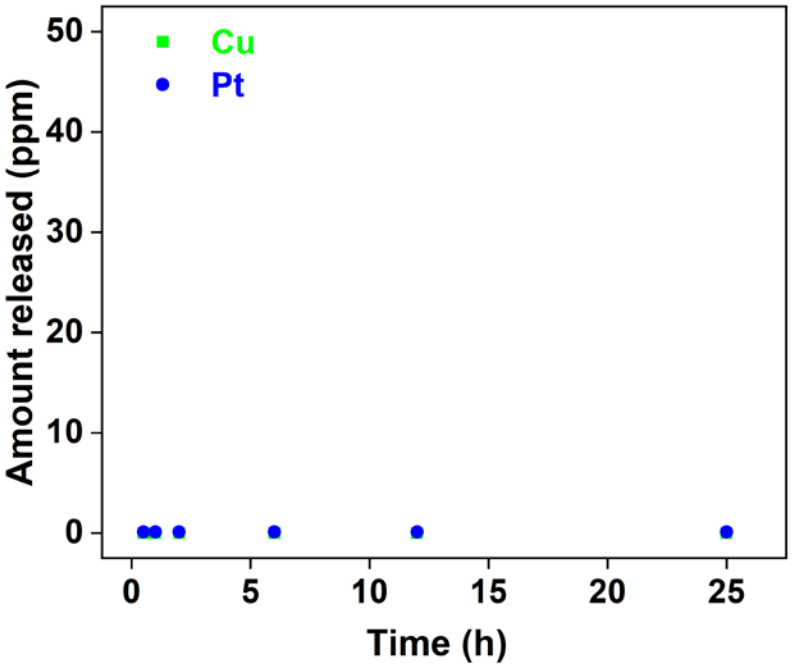

Fig. S14 Cu and Pt release of MOF@Cu/Ru/Pt in PBS solution (pH = 7.4).

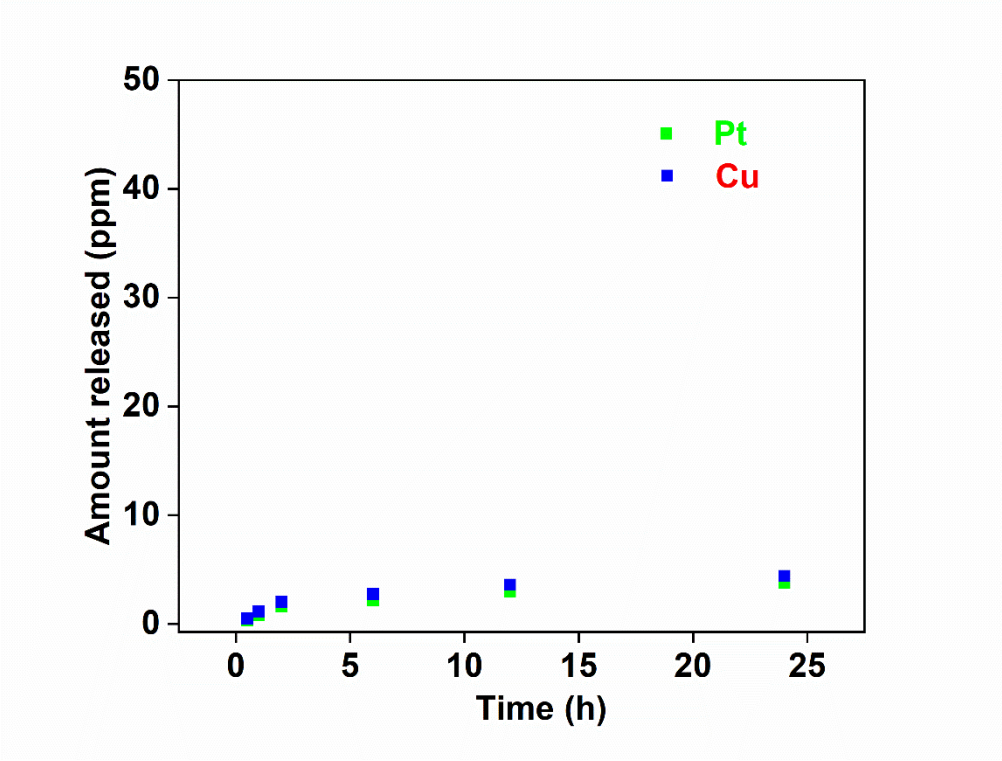

Fig. S15 Metal release of MOF@Cu/Ru/Pt in PBS solution (pH = 5.5).

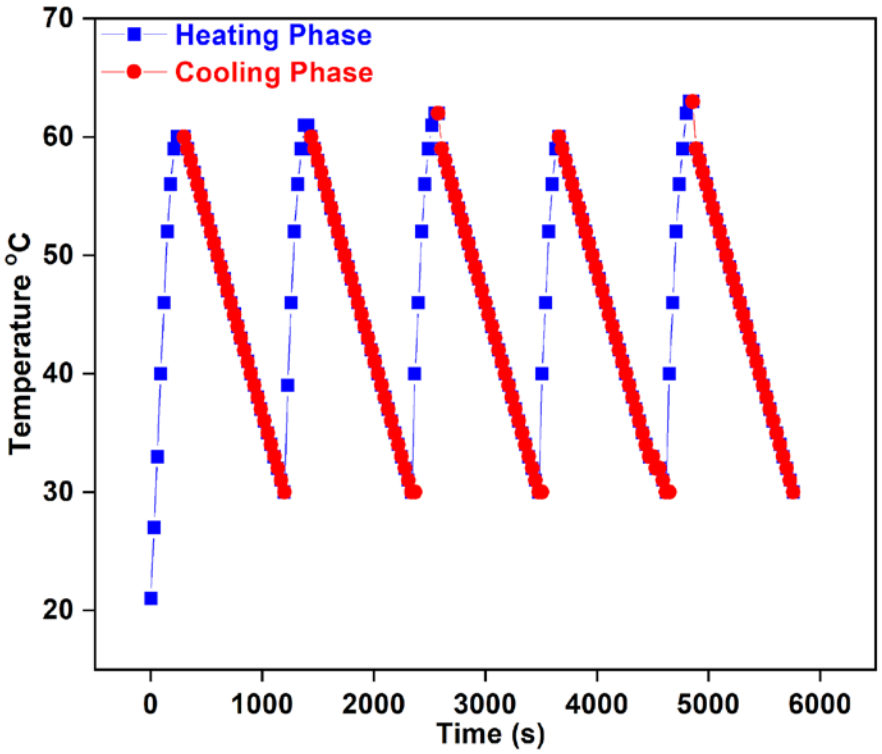

Fig. S16 Heating and cooling curves of MOF@Cu/Ru/Pt for continuous five cycles.

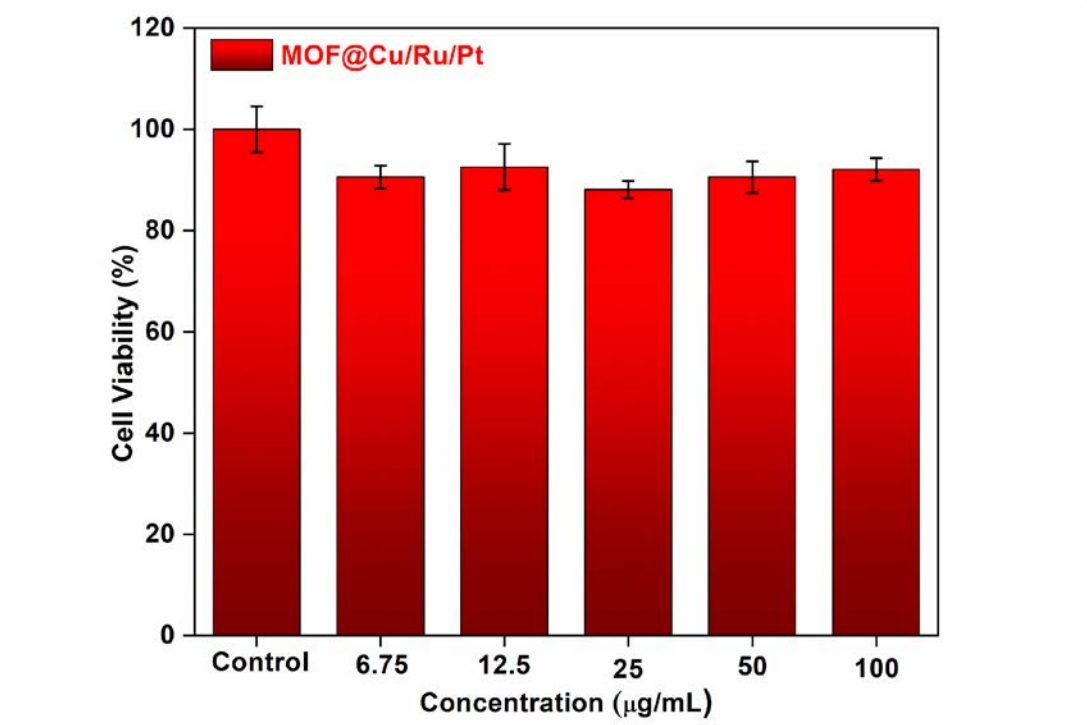

Fig. S17 MTT assays of L929 cells upon incubation with MOF@Cu/Ru/Pt without laser treatment.

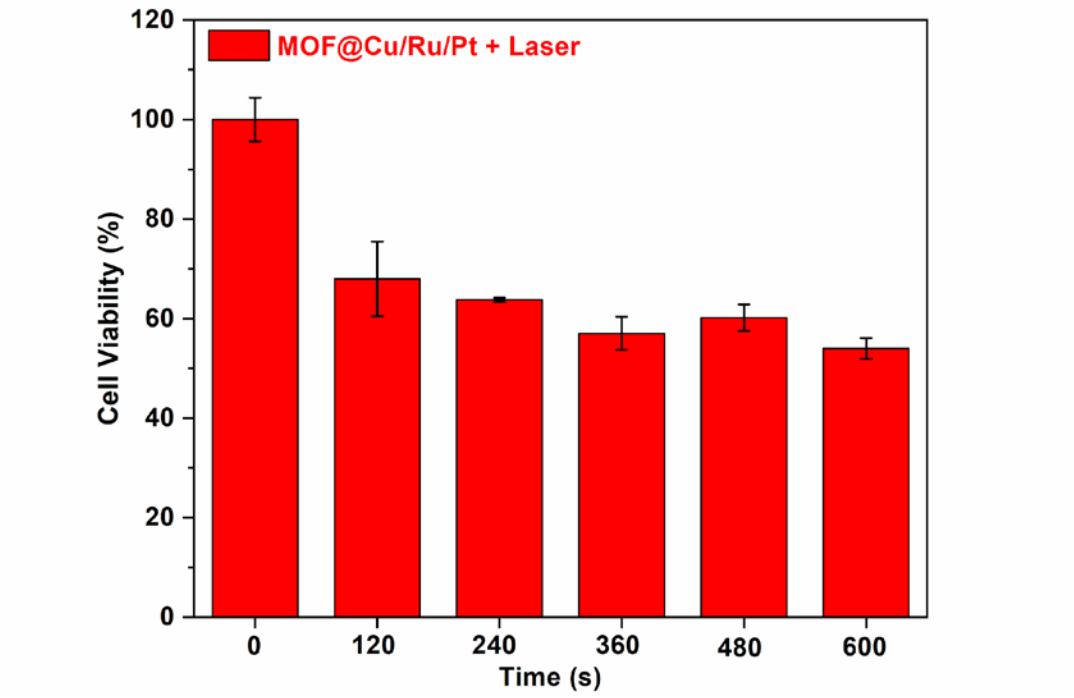

Fig. S18 MTT assays of L929 cells upon incubation with MOF@Cu/Ru/Pt with 808 nm laser irradiation.

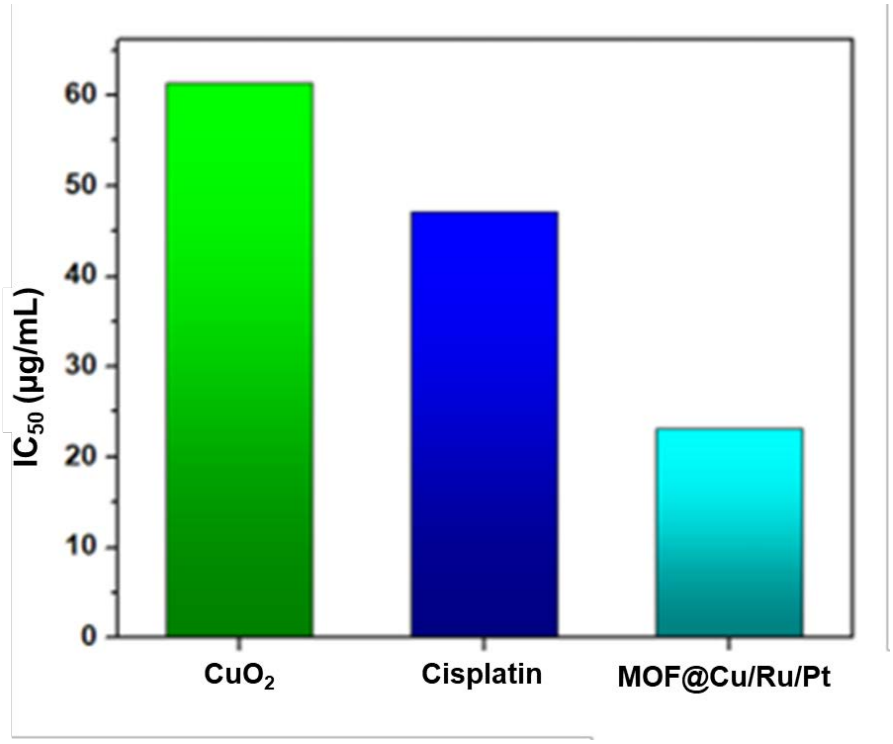

Fig. S19 IC_{50} values of CuO_2, Cisplatin, and MOF@Cu/Ru/Pt.

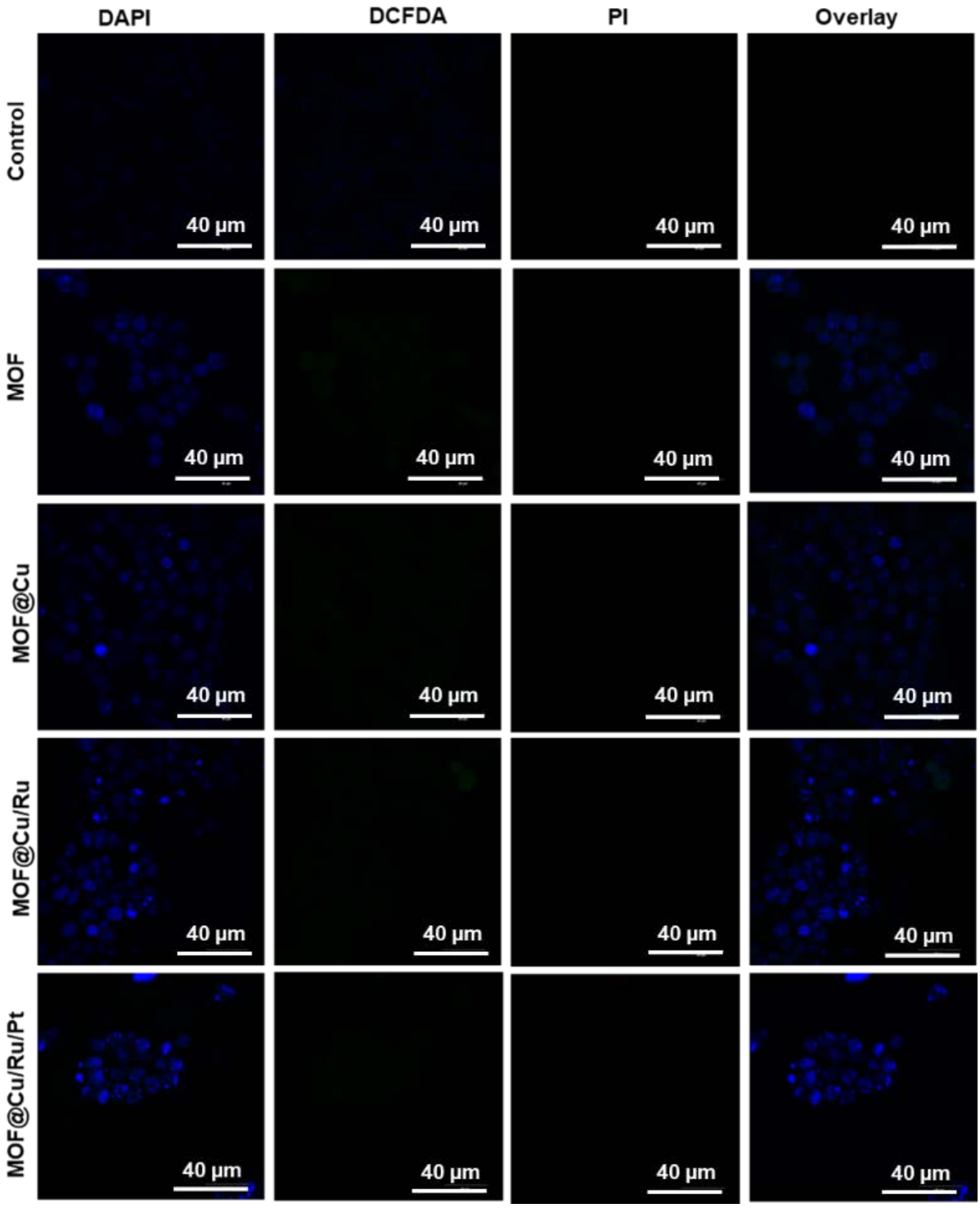

Fig. S20 Live and dead cell assay of 4T1 cells incubated with control, MOF, MOF@Cu, MOF@Cu/Ru, and MOF@Cu/Ru/Pt without laser irradiation, followed by staining with DAPI, DCFDA, and PI.

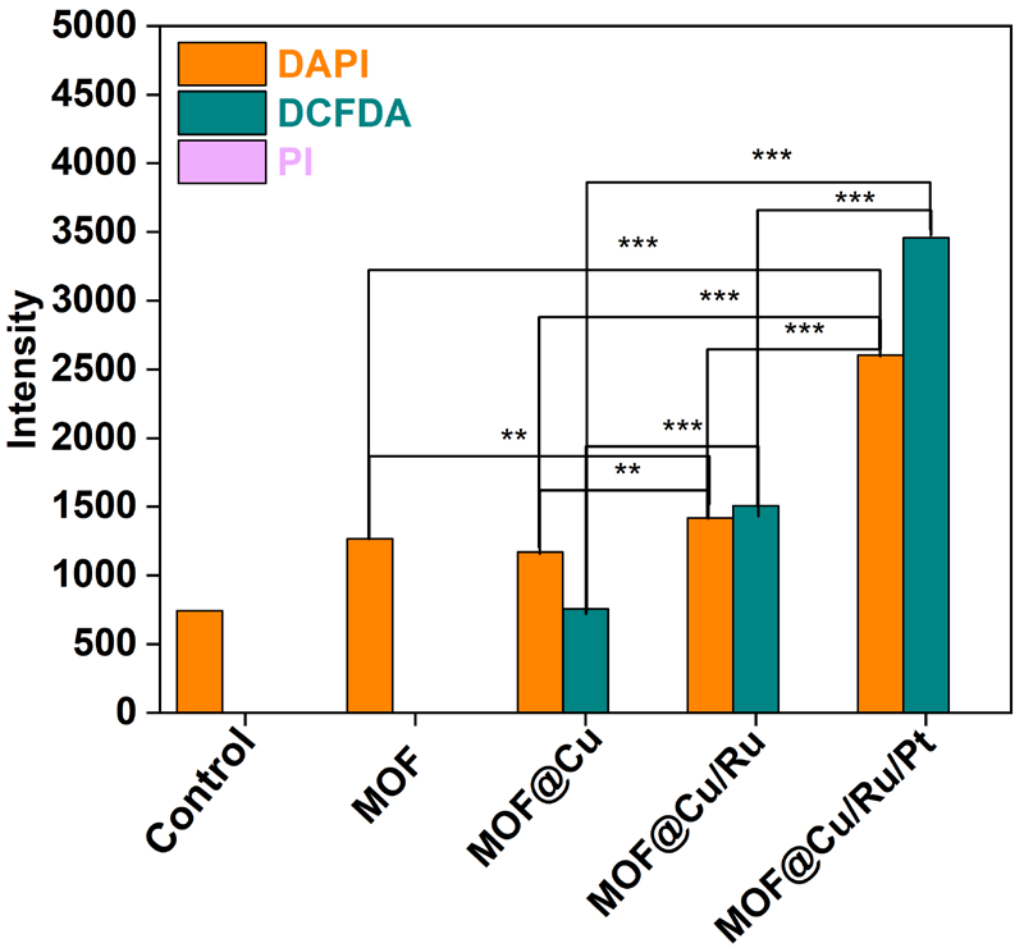

Fig. S21 Fluorescence intensity calculated from Fig. 4b. Statistical significance is indicated as follows: *$p < 0.05$ (significant), **$p < 0.01$ (highly significant), *** $p < 0.001$ (very highly significant).

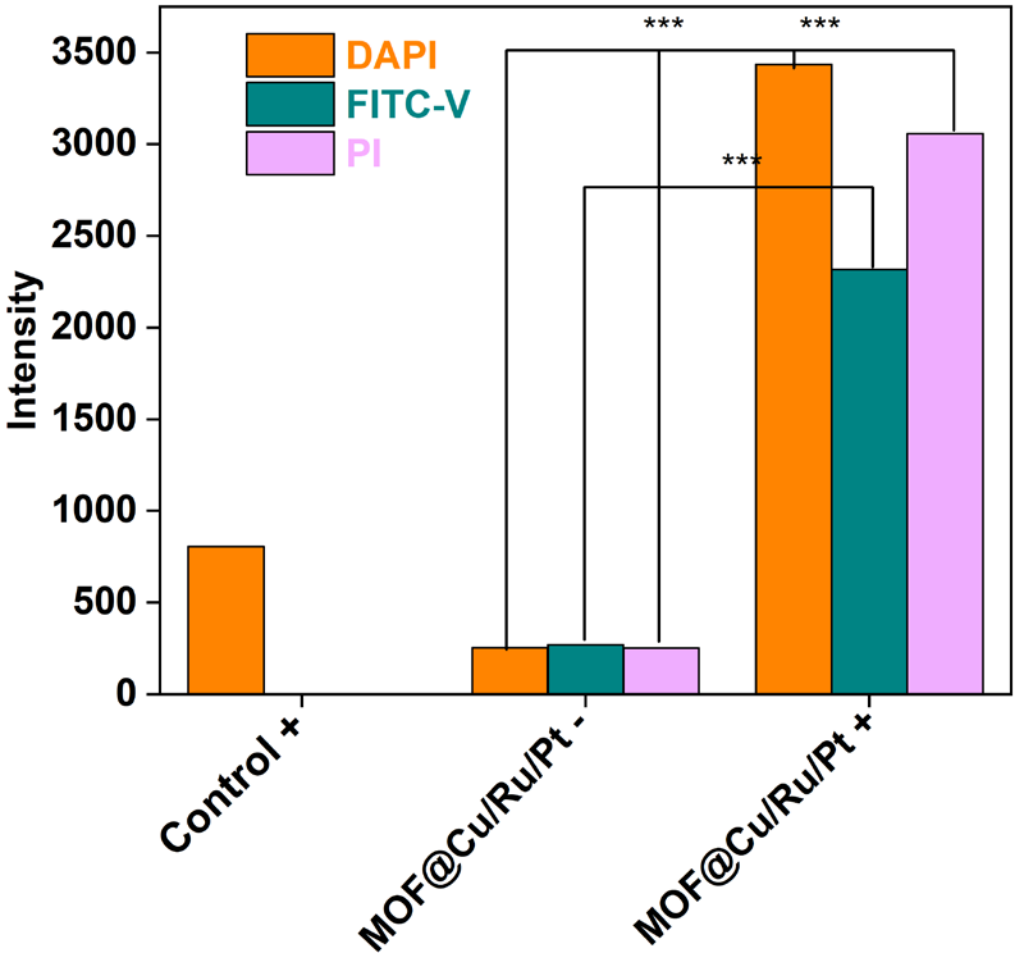

Fig. S22 Fluorescence intensity calculated from Fig. 5. Statistical significance is indicated as follows: *$p < 0.05$ (significant), **$p < 0.01$ (highly significant), *** $p < 0.001$ (very highly significant).

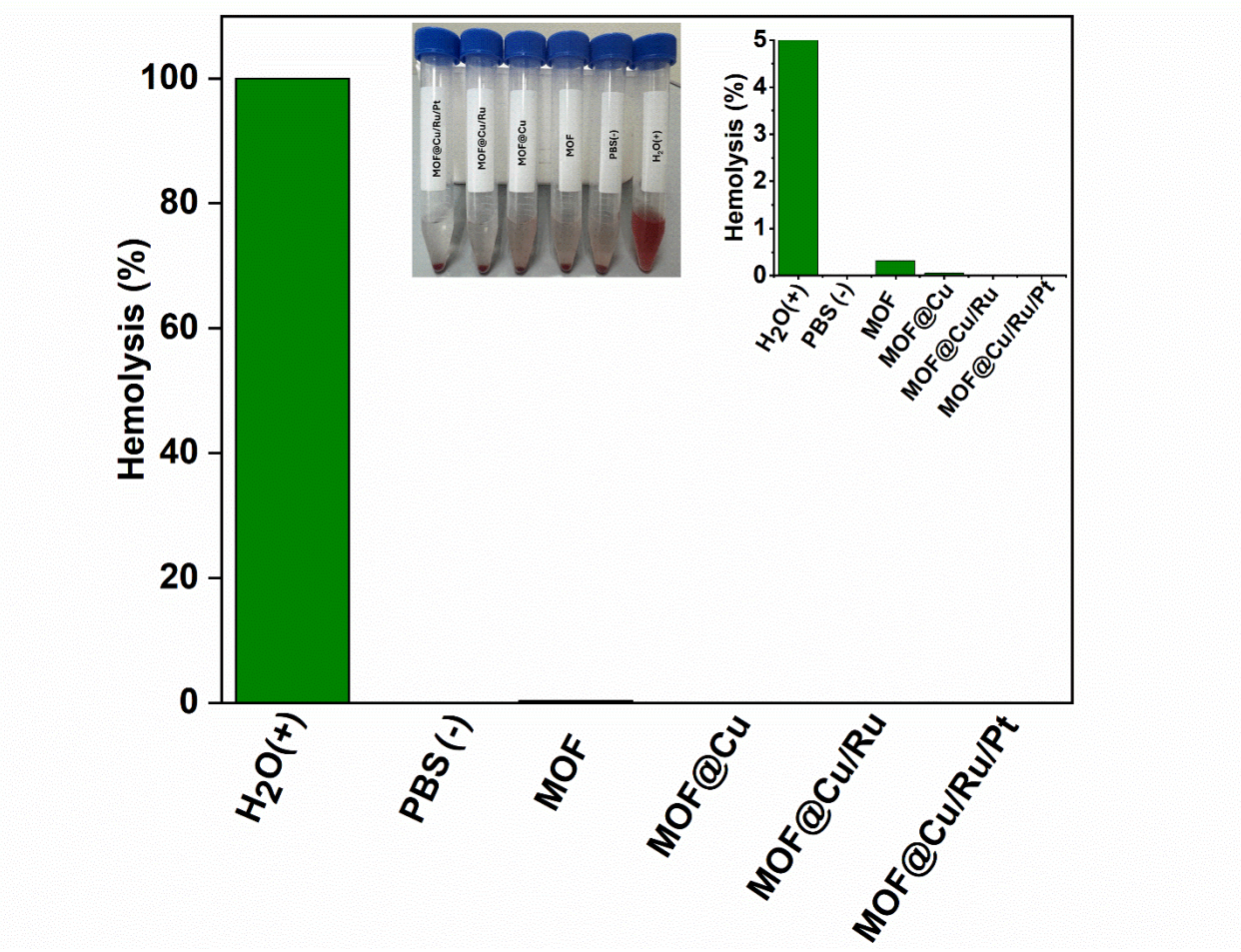

Fig. S23 Hemolysis ratios of MOF, MOF@Cu, MOF@Cu/Ru, and MOF@Cu/Ru/Pt.

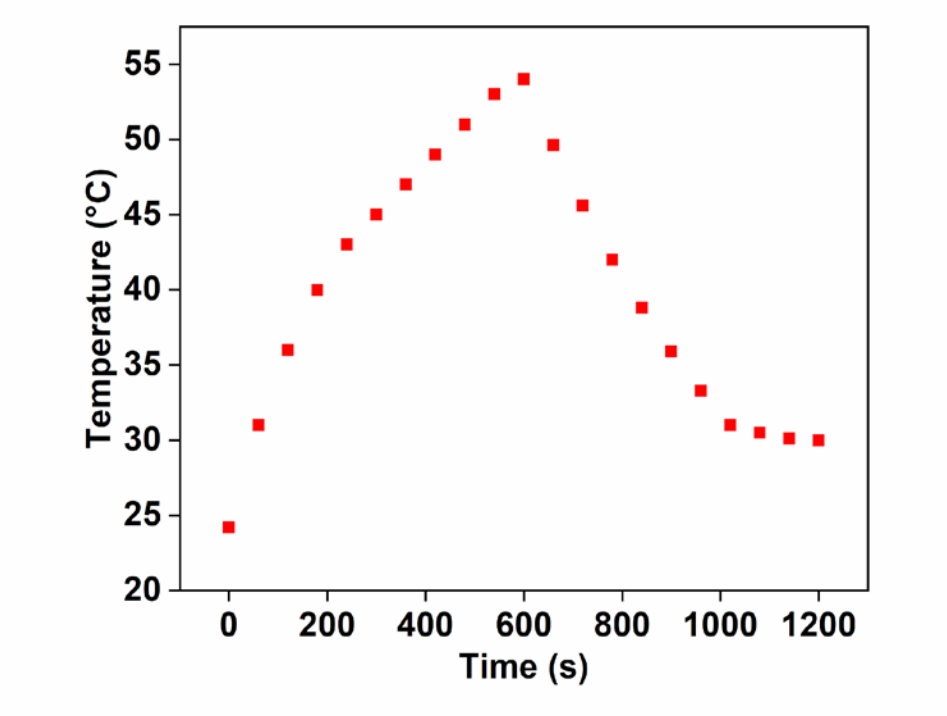

Fig. S24 Temperature rise and fall curves of MOF@Cu/Ru/Pt.

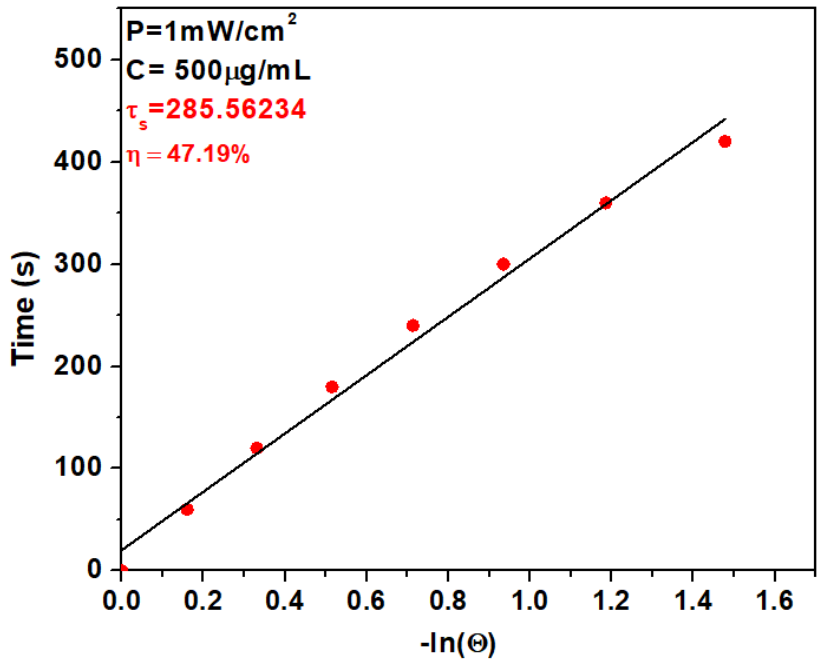

Fig. S25 Plot of cooling time versus -ln(θ) of MOF@Cu/Ru/Pt.

Table S1 Elemental distribution of MOF@Cu/Ru/Pt from SEM-EDS.

Element	Weight %	Atomic %
Cu	23.2	47.5
Ru	2.1	2.7
Pt	74.7	49.9

Table S2 Elemental distribution of MOF@Cu/Ru/Pt from ICP-MS.

Element	Weight %	Atomic %
Cu	50.3	70.5
Ru	16.3	14.3
Pt	33.4	15.2

Table S3 Photothermal conversion efficiency of reported nanomaterials for comparison.

Materials	**Light wavelength (nm)**	**Efficiency (%)**	**Reference**
RuNPs	808	53.2	2
AuNRs	808	87.5	2
Fe_3O_4 NPs	808	19.23	3
CFO@PDA@UiO	808	17.13	4
PDA NPs	665	60.4	5
PDA@UiO-66	808	33.6	6
TiO_{2-x}@POMs	808	37.3	7
GdNDs	808	43.99	8
Cy@ZIF-8	808	33.2	9
LA-AuNR/ZIF-8	808	33	10
CuO_2@MPDA	808	-	11
MOF@Cu/Ru/Pt	808	47	This work

References

1. Y. Lun, L. Lin, F.-P. Huang, P. Zhang and Z. Wang, *Inorg. Chem.*, 2025, **64**, 18950–18959.
2. S. Zhao, X. Zhu, C. Cao, J. Sun and J. Liu, *J. Colloid Interface Sci.*, 2018, **511**, 325–334.
3. J. Zheng, X. Wang, H. Du, R. Zhang, X. Huo, T. Zhou, G. Zhang, F. Wang, Q. Zhou and Z. Zhang, *J. Inorg. Biochem.*, 2025, **262**, 112771.
4. E. Mohammadi, F. Pishbin, A. Ghaee, M. Akrami and F. Rezaei, *ACS Appl. Bio Mater.*, 2025, **8**, 9664–9679.
5. B. Poinard, S. Z. Y. Neo, E. L. L. Yeo, H. P. S. Heng, K. G. Neoh and J. C. Y. Kah, *ACS Appl. Mater. Interfaces*, 2018, **10**, 21125–21136.
6. T. Lin, J. Yang, Y. Li, Y. Cai, X. Zhou, T. Chen and R. Dong, *Adv. Robot. Res.*, DOI: 10.1002/adrr.202500104.
7. X. Li, H. Wu, C. Jiang, J. Zou, Q. Wang, M. Guan, J.-N. Hao, Y. Cao and Y. Li, *Chem. Asian J.*, 2022, **17**, e202200570.
8. F. Li, T. Li, D. Zhi, P. Xu, W. Wang, Y. Hu, Y. Zhang, S. Wang, J. Matula Thomas, J. Beauchamp Norman, W. Ding, L. Yan and B. Qiu, *Biomater.*, 2020, **256**, 120219.
9. Y. Li, N. Xu, J. Zhou, W. Zhu, L. Li, M. Dong, H. Yu, L. Wang, W. Liu and Z. Xie, *Biomater. Sci.*, 2018, **6**, 2918–2924.
10. H. Zhang, Q. Zhang, C. Liu and B. Han, *Biomater. Sci.*, 2019, **7**, 1696–1704.
11. K. Wang, X. Wang, L. Zhang, Y. Tang, J. Zhao, Y. Feng, R. Gao, Y. Hao and X. Tang, *ACS Appl. Mater. Interfaces*, 2024, **16**, 64579–64591.